CSIAM Trans. Appl. Math.
doi: 10.4208/csiam-am.2020-0019

Vol. **1**, No. xx, pp. 1-23
xxx 2020

Modeling and Computation of Nano-Optics

Gang Bao[1], Ricardo Delgadillo[2], Guanghui Hu[3], Di Liu[4,*] and Songting Luo[5]

[1] *School of Mathematical Sciences, Zhejiang University, China.*
[2] *Department of Mathematics, National University of Singapore.*
[3] *Department of Mathematics, University of Macau and UM Zhuhai Research Institute, China.*
[4] *Department of Mathematics, Michigan State University, USA.*
[5] *Department of Mathematics, Iowa State University, USA.*

Received 8 May 2020; Accepted 14 September 2020

Abstract. This work is devoted to a review of our recent studies in the modeling and computation of nano optical devices. Motivated by technological advances at nano scale, to quantitatively understand the mechanism and improve the designing, we make an effort to model nano optical systems involving multiple physical processes across different time and space scales, and develop multiscale and adaptive numerical methods for simulation. Challenges on rigorous analysis of the models and algorithms are also discussed.

AMS subject classifications: 78A45, 81-08, 81V55

Key words: Optical response, nano structures, multi-scale methods, adaptive schemes.

1 Introduction

Recent advances in nano optical technology have been made in a variety of fields such as molecular imaging, optical-mechanical systems, negative-index metamaterials, etc. The study of efficient and accurate numerical methods for multiphysical models of nano scale optical devices has become more important than ever [1]. When size of optical structures reaches sub-micro scale, the energy level for the electron excitation becomes comparable to the wavelength of the incident light. In this case, to faithfully capture light-matter interactions, it is imperative to consider microscopic fields generated by electronic charges in motion. As a complete characterization of the microscopic interaction of light and charged particles, the Quantum Electrodynamics Theory (QED) [2] has been widely used

*Corresponding author. *Email addresses:* baog@math.zju.edu.cn (G. Bao), matrad@nus.edu.sg (R. Delgadillo), garyhu@umac.mo (G. Hu), liudi1@msu.edu (D. Liu), luos@iastate.edu (S. Luo)

with much success in atomic modeling of optical phenomena. However, the fact that QED requires extremely intense computation prohibits it from many applications at meso and nano scales. To avoid the complexity of QED while keeping essential physics, semiclassical models have been recently developed in the form of a nonlocal response theory [3–5], in which the evolution of electromagnetic (EM) field is described continuously using classical Maxwell's equations, and the motion of electrons is treated quantum mechanically by the Schrödinger equation. Compared with QED, the semiclassical model only takes into account averaged quantities, such as certain amplitude and phase, instead of detailed properties, of the statistical ensemble of photons in each mode.

Although the semiclassical approach reduces the computational cost that would otherwise be tremendous in QED, a time dependent many body Schrödinger equation is still involved, for which numerical solutions are prohibitively expensive in many practical situations. A recent effort by the authors [6–12] is to adopt the Time Dependent Current Density Functional Theory (TD-CDFT) [14] to further simplify the semiclassical model and its computation. In the Density Functional Theory (DFT), a one-to-one correspondence (up to an arbitrary constant) between the external potential and the ground state electron density has been proved in the seminal work of Hohenberg and Kohn [15]. Hence, the wavefunction can be obtained as a functional of the electron density, which allows evaluation of all observables of the system. Similar results have been extended to the case of time evolutionary electronic structures in the form of Time Dependent Density Functional Theory (TD-DFT) by Runge and Gross [16]; and later to the situation of external electric and magnetic fields with arbitrary time dependence by Ghosh and Dhara [14] in the form of TD-CDFT, where the current density is introduced as the fundamental variable. A synthetic noninteracting many body system under an effective external potential, referred as the Kohn-Sham (KS) system [17], is designed to calculate electron and current densities, which greatly simplifies the computation by reducing dimension of the problem. In the KS system, many body effects are included via so called exchange-correlation (xc) potentials.

The incorporation of TD-CDFT into the framework of the semiclassical optical response theory leads to a system formulated as coupled Maxwell-Kohn-Sham (MKS) equations (also see [18–20] for similar systems). Challenges still remain in numerically solving the MKS system when applied to nano optical applications of interest. First of all, the MKS system has a multiscale nature due to space and time scale separations between electrodynamics and electronic motions, for the fact that the EM field spreads the whole medium domain while electrons are confined in nano scale structures. It is recently observed that at nano scale, the speed of photon excited electrons is about 375 times slower than the speed of light [21]. Direct and uniform space and time discretizations of the MKS system will result in very large and ill-conditioned equations. The situation becomes more subtle when it comes to non-adiabatic coupling of different physical processes, e.g., light driven molecular motions and transitions under strong external fields, where the dynamics can be highly nonlinear and a large number of degrees of freedom is needed to resolve details across all scales.

In this paper, we discuss recent progress and ongoing efforts on the multiscale and adaptive methods for multiphysical models of nano optical structures, as well as theoretical issues raised by modeling and simulation. There are two major progress. Firstly, in the regime of linear responses, we derived a system of linear equations for simultaneously determining the EM fields, and the current and electron densities, for nano optical structures. The zero eigenvalue problem of the linear system corresponds to the resonant frequencies and self-sustaining modes of the nano optical response. To deal with disparate space scales of the system, a multiscale scheme is proposed [6,7] to solve the system self-consistently by allowing communications between the macro solver for Maxwell's equations and the micro solver for the Kohn-Sham equations. More recently, we apply the method to study light driven nano devices by further incorporating Ehrenfest molecular dynamics [8]. Secondly, aiming at nonlinear problems involving strong attosecond $(10^{-18}s)$ laser pulses and metallic nano particles, we have developed several adaptive techniques for the time dependent Density Functional Theory [9–12], based on a posteriori error estimates of Finite Element Methods for the time dependent Kohn-Sham equation, and more recently a novel spectral method [13] in the semiclassical regime using a Fourier integral operator commonly known as the Frozen Gaussian approximation (FGA) ansatz.

The paper is organized as follows. In Section 2, we will first introduce nano optical systems that motivate the research. Details on the multiscale computation of linear nano optical responses and numerical methods for nonlinear TD-DFT are presented in Section 3 and Section 4, respectively. Finally, we discuss ongoing efforts on applications of the numerical schemes to novel nano optical structures, as well as challenges for further analysis of the models and algorithms.

2 Motivating examples of nano optical systems

In this section, we present some recent advances in optical nano technology. A quantitative investigation will provide the badly needed guidance for optimal designs and novel applications.

2.1 Photon driven nano devices

Optically manipulated nano devices have attracted a lot of recent interest with applications in solar energy harvesting, molecular sensing and non-invasive regulation of intracellular reactions [22, 23]. Fig. 1 shows two such examples: (a) a photoresponsive DNA nanomotor enhanced by silver nanowires, and (b) a laser driven micromotor in a fluid environment. Illuminated by UV and visible lights, the DNA nanomotors (a) can switch back and forth between 'open' and 'loop' states, thereby converting photon energy to mechanical energy [24]. The mechanism is facilitated by incorporating azobenzene moieties that can change the conformational structure through the cis-trans isomerisation. The efficiency of the conversion can be significantly enhanced by a plasmonic near-field

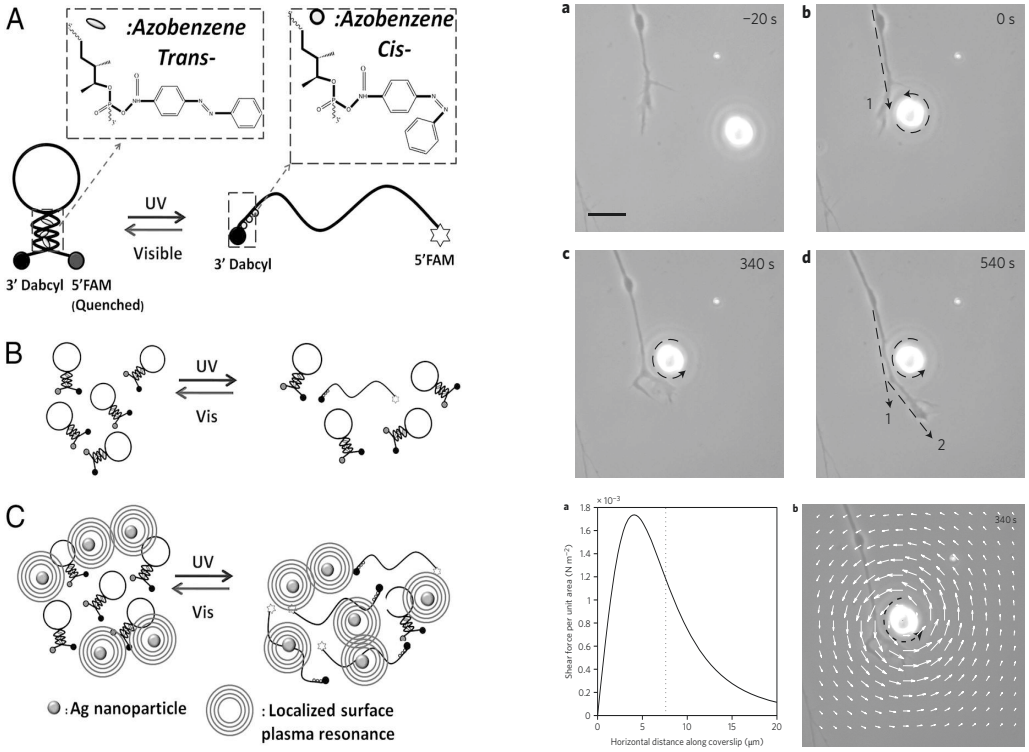

(a) Photoresponsive DNA nanomotors [24] (b) Photon driven micromotors [26]

Figure 1: Photon driven nano and micro devices.

coupling with silver nanoparticles, due to the spectral overlap between the azobenzene absorption band and plasmonic resonances of silver nanowires. Recent applications include photon manipulated drug release from nanocontainers, building nanostructures using photonic energy, a photocontrolled molecular beacon for mRNA detection in living cells [25], etc. The micromotors (b) are birefringent vaterite particles with positions being controlled by a linearly polarized laser beam. Meanwhile, a circularly polarized laser with an angular momentum can cause the trapped beads to spin, and generate a localized microfluidic flow. Also shown in the figure is a growing nerve fibre from the goldfish retinal ganglion cell. The direction of axonal growth can be precisely manipulated by changing rotational direction and position of the optically driven micromotor [26]. A more recent example is the light propulsion of bulk graphene material [27], which has great potential for applications in solar sail and space transportation. The modeling and simulation of such systems will obviously require the coupling of light scattering and transmission, electronic excitation, as well as molecular motion.

2.2 Optical response to strong laser pulses

Recent development in laser technology has led to reliable production of attosecond $(10^{-18}s)$ pulses, which enables ultrafast and highly nonlinear photon excitations and allows real time molecular orbital imaging [28, 29]. In high order harmonic generations (HHG), the spectrum of the response light can extend over many orders of magnitudes at multiples of the driving frequency. What is of great practical interest is the optimal control of the efficiency and spectral characteristics of the harmonic radiation by modifying the incident pulse. Time Dependent Density Functional Theory (TD-DFT) has been adopted as a major tool for investigating physics with intense laser pulses, especially for HHG and multiphoton ionizations [30, 31]. Much of the effort has been focused on developing appropriate exchange-correlation functionals that reproduce experimental observations. Efficient numerical schemes that can capture the femtosecond dynamics will be greatly useful to the understanding of the mechanism and interpretation of data.

2.3 Metal nano structures

Metal nano structures have attracted a great deal of interest for being able to significantly enhance the local field due to light induced surface plasmons [32], and further affect optical scattering of molecular structures, which has led to successful applications in photovoltaics, sensing, spectroscopy and metamaterials [33, 34]. Theoretical efforts on understanding nano plasmonic systems have been focused on the quantum effects as a result of the reduced size, that can not be captured by macroscopic electrodynamics. DFT/TD-DFT based approaches for modeling optical properties of metal nano structures have the advantage of numerically and (relatively) theoretically tractable, especially in the regime of linear responses [35]. The difficulty lies in the nonlinear effects, which will require not only time domain simulations for interactions between a large number of ions and electrons, but also model simplification and validation for nano scale systems [36].

3 Multiscale computation of light driven molecular dynamics

In this section, we present results for the Maxwell-Ehrenfest-Kohn-Sham system that couples the evolution of the electromagnetic fields, the molecular motion and the electronic excitation for the study of light driven nano devices. Details of the derivation and more numerical results can be found in [6–8].

3.1 Semiclassical theory

In the semiclassical theory [3] of nano optics, the evolution of the EM fields is determined by Maxwell's equations in terms of the vector and scalar potentials $\{\mathbf{A},\phi\}$ under the

Coulomb gauge $\nabla\cdot\mathbf{A}=0$ such that

$$\begin{aligned}&\frac{1}{c^2}\frac{\partial^2\mathbf{A}(\mathbf{r},t)}{\partial t^2}-\nabla^2\mathbf{A}(\mathbf{r},t)+\frac{1}{c}\frac{\partial(\nabla\phi(\mathbf{r},t))}{\partial t}=\frac{4\pi}{c}\mathbf{j}(\mathbf{r},t),\\&-\nabla^2\phi(\mathbf{r},t)=4\pi\rho(\mathbf{r},t),\end{aligned}\tag{3.1}$$

where c is the speed of light in vacuum, and $\mathbf{j}$ and ρ are the current and charge densities. Meanwhile, quantum mechanically, the motion of a system of N charged particles is governed by the time dependent Schrödinger equation [2]:

$$\imath\hbar\frac{\partial\Psi(\mathbf{r}_1,\cdots,\mathbf{r}_N,t)}{\partial t}=H\Psi(\mathbf{r}_1,\cdots,\mathbf{r}_N,t),\tag{3.2}$$

where $\imath=\sqrt{-1}$, $\hbar$ is the reduced Planck constant, and the general nonrelativistic Hamiltonian takes the form

$$H\big(\{\mathbf{r}_l\},\{\mathbf{p}_l\},t\big)=\sum_{l=1}^{N}\frac{1}{2m_l}\Big[\mathbf{p}_l-\frac{e_l}{c}\mathbf{A}(\mathbf{r}_l)\Big]^2+\frac{1}{2}\sum_{l\neq l'}\frac{e_le_{l'}}{|\mathbf{r}_l-\mathbf{r}_{l'}|},\tag{3.3}$$

with e_l, m_l, $\mathbf{r}_l$ and $\mathbf{p}_l$ being the charge, mass, coordinate and conjugate momentum of the l^{th} particle, respectively. Note that we are not separating the positive and negative charges right now. The initial state Ψ_0 before the incident light is applied is assumed to be the ground state. The current and charge densities $\{\mathbf{j},\rho\}$ can be computed as expectations with respect to the solution of the Schrödinger equation:

$$\mathbf{j}(\mathbf{r},t)=\langle\Psi|\hat{\mathbf{j}}|\Psi\rangle,\qquad\rho(\mathbf{r},t)=\langle\Psi|\hat{\rho}|\Psi\rangle,\tag{3.4}$$

with the current and charge density operators $\{\hat{\mathbf{j}},\hat{\rho}\}$ given by

$$\begin{aligned}&\hat{\mathbf{j}}=\sum_{l=1}^{N}\frac{e_l}{2m_l}\Big[\mathbf{p}_l\mathrm{I}(\mathbf{r}-\mathbf{r}_l)+\mathrm{I}(\mathbf{r}-\mathbf{r}_l)\mathbf{p}_l\Big]-\sum_{l=1}^{N}\frac{e_l^2}{m_lc}\mathbf{A}(\mathbf{r}_l,t),\\&\hat{\rho}=\sum_{l=1}^{N}e_l\mathrm{I}(\mathbf{r}-\mathbf{r}_l),\end{aligned}\tag{3.5}$$

where $\mathrm{I}(\cdot)$ is the Dirac delta function. In the semiclassical model, the light-matter interaction is completely described by $(\mathbf{A},\phi)$ and Ψ as a coupled system of Maxwell's equations (3.1) and Schrödinger equation (3.2), through the current and charge densities by (3.4). Therefore the system must be solved self-consistently.

3.2 Ehrenfest molecular dynamics

To incorporate the molecular motion, we adopt the Ehrenfest molecular dynamics. We first separate the electronic and nuclear degrees of freedom by denoting the positions of

the electrons and nuclei with $\vec{\mathbf{r}}=(\mathbf{r}_1,\cdots,\mathbf{r}_{N_e})$ and $\overrightarrow{\mathbf{R}}=(\mathbf{R}_1,\cdots,\mathbf{R}_{N_n})$, where N_e and N_n are the total number of electrons and nuclei. The electronic and nuclear wavefunctions are given by ψ and Φ, respectively. We denote by $(e,m,\mathbf{r}_l,\mathbf{p}_l)$ the charge, mass, coordinate, and conjugate momentum of l^{th} electron, while $(Z_k,M_k,\mathbf{R}_k,\mathbf{P}_k)$ represent the corresponding variables for the k^{th} nucleus. The Coulomb interactions can be partitioned into

$$\begin{aligned} &W_{ee}(\vec{\mathbf{r}})=\frac{1}{2}\sum_{j\neq k}^{N_e}\frac{e^2}{|\mathbf{r}_j-\mathbf{r}_k|}, \qquad W_{nn}(\overrightarrow{\mathbf{R}})=\frac{1}{2}\sum_{j\neq k}^{N_n}\frac{Z_jZ_k}{|\mathbf{R}_j-\mathbf{R}_k|},\\ &W_{en}(\vec{\mathbf{r}},\overrightarrow{\mathbf{R}})=\sum_{j=1}^{N_e}\sum_{k=1}^{N_n}\frac{eZ_k}{|\mathbf{r}_j-\mathbf{R}_k|}. \end{aligned} \tag{3.6}$$

We assume the following single determinant ansatz for the solution of (3.2):

$$\Psi(\vec{\mathbf{r}},\overrightarrow{\mathbf{R}},t)=\psi(\vec{\mathbf{r}},t)\Phi(\overrightarrow{\mathbf{R}},t)\exp\left(\frac{\iota}{\hbar}\int_{t_0}^{t}\langle H_e\rangle_{\vec{\mathbf{r}},\overrightarrow{\mathbf{R}}}\right), \tag{3.7}$$

where $\langle\cdot\rangle_z$ denotes expectation with respect to z variable and

$$H_e=\sum_{l=1}^{N_e}\frac{1}{2m}\left[\mathbf{p}_l-\frac{e}{c}\mathbf{A}(\mathbf{r}_l)\right]^2+W_{ee}+W_{nn}+W_{en}. \tag{3.8}$$

The motion of nuclei is further approximated with the mean field approximation by assuming that the nuclear wavefunction has the WKB ansatz [37]

$$\Phi(\overrightarrow{\mathbf{R}},t)\approx A(\overrightarrow{\mathbf{R}},t)e^{\iota S(\overrightarrow{\mathbf{R}},t)/\hbar}, \quad \text{as } \hbar\to 0, \tag{3.9}$$

where A is the amplitude and S is the phase. It can be shown [8,37] that under (3.7) and (3.9), the motion of electrons is determined by the electronic Schrödinger equation

$$\iota\hbar\frac{\partial\psi(\vec{\mathbf{r}},t)}{\partial t}=\left(\sum_{l=1}^{K}\frac{1}{2m}\left[\mathbf{p}_l-\frac{e}{c}\mathbf{A}(\mathbf{r}_l)\right]^2+\langle W_{ee}+W_{nn}+W_{en}\rangle_{\mathbf{R}}\right)\psi(\vec{\mathbf{r}},t), \tag{3.10}$$

and the motion of nuclei is determined by Hamiltonian dynamics

$$M_k\frac{d^2\mathbf{R}_k}{dt^2}=\frac{-Z_k}{c}\left(\frac{\partial\mathbf{A}(\mathbf{R}_k,t)}{\partial t}\right)-\nabla_{\mathbf{R}_k}\left(W_{nn}+\int\rho_e(\mathbf{r},t)W_{sn}(\mathbf{r},\overrightarrow{\mathbf{R}})d\mathbf{r}\right), \tag{3.11}$$

for $k=1,\cdots,N_n$, and

$$W_{sn}(\mathbf{r},\overrightarrow{\mathbf{R}})=\sum_{k=1}^{N_n}\frac{eZ_k}{|\mathbf{r}-\mathbf{R}_k|}. \tag{3.12}$$

The coupled equation (3.10) and (3.11) is referred as Ehrenfest dynamics of electrons and nuclei.

3.3 Time dependent current density functional theory (TD-CDFT)

For computing the electronic charge and current densities, denoted as $\{\rho_e, \mathbf{j}_e\}$, instead of solving the many body Schrödinger equation (3.10), TD-CDFT is adopted. The advantage of TD-CDFT is the greatly reduced computational cost by restricting to the charge and current densities that are functions of only three dimensional (3D) spatial variables. For a system satisfying the time dependent Schrödinger equation (3.10), a system of time dependent Kohn-Sham (TDKS) equations can also be constructed in TD-CDFT [14] in the following form:

$$\imath\hbar\frac{\partial\psi_l(\mathbf{r},t)}{\partial t} = H_{KS}\psi_l(\mathbf{r},t), \quad \text{for } l=1,\cdots,N_e, \tag{3.13}$$

with the Hamiltonian

$$H_{KS}(\mathbf{r},\mathbf{p},t) = \frac{1}{2m}\left[\mathbf{p}-\frac{e}{c}\mathbf{A}_{KS}(\mathbf{r},t)\right]^2 + v_{KS}(\mathbf{r},t). \tag{3.14}$$

The scalar time dependent KS potential is given by

$$v_{KS}(\mathbf{r},t) = v(\mathbf{r},t)+v_H(\mathbf{r},t)+v_{xc}(\mathbf{r},t), \tag{3.15}$$

where v is the external potential due to nuclear attraction, and v_H is the Hartree potential given as

$$v_H(\mathbf{r},\mathbf{t}) = e\int\frac{\rho_e(\mathbf{r}',t)}{|\mathbf{r}-\mathbf{r}'|}d\mathbf{r}'. \tag{3.16}$$

The exchange-correlation (xc) potential v_{xc} contains the many body effects as a functional of ρ_e. The vector KS potential has the form:

$$\mathbf{A}_{KS}(\mathbf{r},t) = \mathbf{A}(\mathbf{r},t)+\mathbf{A}_{xc}(\mathbf{r},t), \tag{3.17}$$

with $\mathbf{A}$ being the vector potential of the EM field, and $\mathbf{A}_{xc}$ being the vector xc-potential that is a functional of the current density $\mathbf{j}_e$. Once the KS system (3.13) is solved, we can compute the electronic charge density ρ_e by

$$\rho_e(\mathbf{r}) = \sum_{l=1}^{N_e} e f_l|\psi_l(\mathbf{r})|^2, \tag{3.18}$$

where f_l is the occupation number of orbital ψ_l, and the electronic current density is given by

$$\begin{aligned}\mathbf{j}_e(\mathbf{r},t) = &-\frac{\imath\hbar e}{2m}\sum_{l=1}^{N_e} f_l\left[\psi_l^*(\mathbf{r},t)\nabla\psi_l(\mathbf{r},t)-\psi_l(\mathbf{r},t)\nabla\psi_l^*(\mathbf{r},t)\right]\\ &-\frac{e}{mc}\rho_e(\mathbf{r},t)\mathbf{A}_{KS}(\mathbf{r},t).\end{aligned} \tag{3.19}$$

The initial condition can be obtained by solving the ground state Kohn-Sham (KS) system

$$H_0\psi_l(\mathbf{r})=\epsilon_l\psi_l(\mathbf{r}),\quad \text{for } l=1,\cdots,N_e, \tag{3.20}$$

with

$$H_0(\mathbf{r},\mathbf{p})=\frac{1}{2m}\mathbf{p}^2+v_{KS}(\mathbf{r}). \tag{3.21}$$

In practice, both the scalar xc-potential v_{xc} and the vector xc-potential $\mathbf{A}_{xc}$ need to be approximated. For v_{xc}, the local density approximation (LDA) is chosen for for the ground states, and the adiabatic local density approximation (ALDA) is used in time dependent case, with parametrization of Vosko, Wilk, and Nusair (VWN) [38]. For the vector xc-potential $\mathbf{A}_{xc}$, the Vignale-Kohn (VK) functional [39] is adopted.

3.4 The coupled Maxwell-Ehrenfest-Kohn-Sham (MEKS) system

The coupled system that is capable of describing the interactions between the induced EM field, the molecular motion and the electronic excitation consists of Maxwell's equations (3.1) for the EM field, the Ehrenfest dynamics for the nuclei (3.11), and time dependent Kohn-Sham system for the electrons (3.13). We refer to this system as Maxwell-Ehrenfest-Kohn-Sham (MEKS) equations which must be solved simultaneously. On the right hand side of Maxwell's equation (3.1), the current and charge densities are partitioned into the electronic and nuclear contributions such as

$$\mathbf{j}(\mathbf{r},t)=\mathbf{j}_e(\mathbf{r},t)+\mathbf{j}_n(\mathbf{r},t),\quad \rho(\mathbf{r},t)=\rho_e(\mathbf{r},t)+\rho_n(\mathbf{r},t).$$

The electronic current and charge densities can be obtained by the KS equation (3.13), and the current and charge densities due to nuclear motion, denoted as $(\mathbf{j}_n,\rho_n)$, are given as

$$\rho_n(\mathbf{R},t)=\sum_{k=1}^{N_n}Z_k\mathrm{I}(\mathbf{R}-\mathbf{R}_k),\quad \mathbf{j}_n(\mathbf{R},t)=\sum_{k=1}^{N_n}Z_k\mathbf{v}_k\mathrm{I}(\mathbf{R}-\mathbf{R}_k), \tag{3.22}$$

with $\mathbf{v}_k=\frac{d\mathbf{R}_k}{dt}$. The so obtained MEKS system is multiphysical in nature, as a result of the coupling of physical processes at different time and space scales. It also poses a numerical challenge due to well separated scales, which will lead to a stiff system if one uses direct discretization.

To investigate the resonance effects of light on the molecular structure, we consider the linear response regime by treating the incident light as resonant perturbations driving the system away from the local minimum of the molecular energy landscape. To this end, we assume the nuclei are at equilibrium position before the incident light is switched on. In particular, tackling the system within the linear response regime allows us to solve the coupled system in the frequency (ω) domain. To identify the resonant condition for the nano optical mechanical system, we reformulate the coupled system in a compact form with the $\mathcal{P}$-matrix notation and define the resonant frequencies as solutions of an

eigenvalue problem. As in [40, 41], we adopt the following spectral expansion of the unknowns for the linearized MEKS system:

$$\begin{aligned}\delta\mathbf{j}_e(\mathbf{r},\omega)&=\sum_{ia}\frac{\omega f_i}{\epsilon_i-\epsilon_a}\psi_i(\mathbf{r})\mathbf{j}_p\psi_a(\mathbf{r})\mathcal{P}_{ia}(\omega),\\ \delta\rho_e(\mathbf{r},\omega)&=-\sum_{ia}f_i\psi_i(\mathbf{r})\psi_a(\mathbf{r})\mathcal{P}_{ia}(\omega),\end{aligned}\tag{3.23}$$

where i and a indicate occupied and unoccupied ground state KS orbitals respectively (hereafter, we use i,j for occupied orbitals and a,b for unoccupied orbitals). $\mathcal{P}_{ia}(\omega)$ is the spectral coefficient for each corresponding orbital. The paramagnetic current density operator $\mathbf{j}_p$ is defined as $\mathbf{j}_p=-\iota(\nabla-\nabla^\dagger)/2$, with $\nabla^\dagger$ acting on the term to the left. We can also write $(\delta\mathbf{A},\delta\phi,\delta\mathbf{R}_k,\delta\rho_n,\delta\mathbf{j}_n)$ as linear expansions in terms of (ψ_i,ψ_a) and a linear system for the coefficient matrix $\mathcal{P}$ (see [7, 8] for details) can be obtained based on the linearized MEKS system such that

$$\big(\mathbf{S}(\omega)-\omega^2\mathbf{I}\big)\mathcal{P}=\mathcal{F}(\omega),\tag{3.24}$$

where $\mathbf{S}(\omega)$ is a coefficient matrix and $\mathcal{F}(\omega)$ depends on the incident light, both being functions in terms of ω. The resonant frequency can be determined by the nonlinear eigenvalue problem

$$\det\big(\mathcal{S}(\omega)-\omega^2\mathbf{I}\big)=0.\tag{3.25}$$

The linearized Maxwell-Ehrenfest-Kohn-Sham system avoids the numerical challenge from multiple time scales by solving the system in the frequency domain, but it still inherits the spacewise multiscale nature such that the EM fields extend on the macroscopic domain, while the molecular and electronic structures vary in a microscopic region. A direct discretization of the system with a uniform mesh will lead to a stiff matrix that is numerically ill-conditioned. In [7], we introduced a multiscale scheme in which a macro solver for the EM field is performed in a larger domain partitioned with coarse meshes, while a micro solver for the electronic and molecular dynamics is conducted on a refined mesh covering a smaller domain enclosing the optical device. The coupling of the macro and micro solvers is achieved through self-consistent iterations. Linear interpolation is used for the communication between numerical solutions of the micro and macro solvers.

3.5 Numerical example: Surface plasmon enhancement

Numerical experiments are conducted through the coupled metal nano particles and molecular systems. As demonstrated in Fig. 2, we present here one example such that *trans*-Azobenzene is situated between two Gold nano particles of radius 30 nm that are 2 nm apart. The Lorentz-Drude model for metal nano particles is used with parameters adopted from [42]. The Maxwell's equations are solved with hybrid nodal-edge element methods with absorbing boundary conditions [43]. Fig. 2 shows intensity of the total EM field with the incident light shed in the y direction and polarized in the x direction.

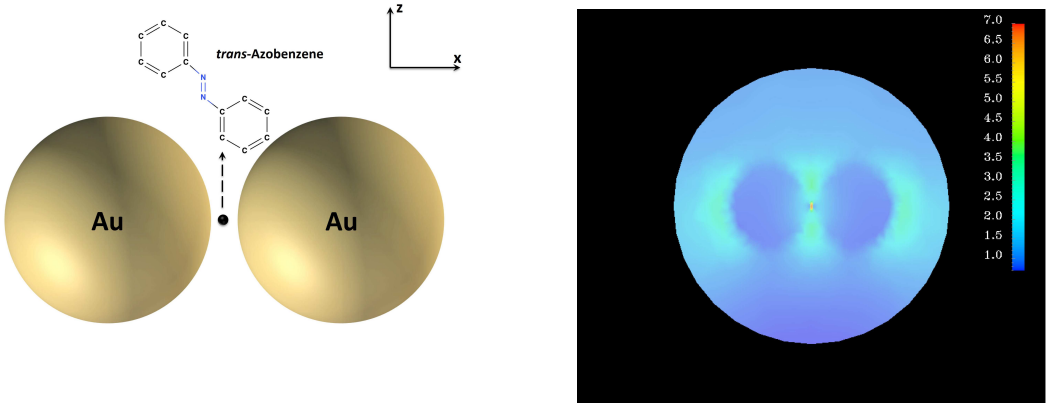

(a) Gold nano particles + molecule system (b) Intensity of the EM field

Figure 2: Gold nano particles and *trans*-Azobenzene system. (a) *trans*-Azobenzene is situated between the two Gold nano particles of radius 30 nm that are 2 nm apart. (b) The intensity of the total EM field projected on the xz plane is demonstrated. The incident field with magnitude 1 and frequency $\omega=0.13$ (a.u.) is shed in the positive y direction with polarization along the positive x direction.

The computational domain for the Maxwell's equations is centered at the molecule with radius 100nm. The domain is discretized with 103317 tetrahedra and 17530 nodes. We remark that in order to incorporate the multiple space scales, the mesh at the molecule is refined while the mesh far away from the molecule is relatively coarsened. The computed lowest eigenfrequency is approximately 0.143 (a.u.) (about 318 nm). Choosing the tolerance of relative residual reduction for solving Maxwell equations to be $\mathcal{O}(10^{-8})$, the CPUtime on a Dell 2.66G workstation is 2.08×10^4 seconds (2.41 days).

4 Numerical methods for time dependent density functional theory

To study highly nonlinear dynamics of large scale electronic structures in the non-perturbative regime, the time domain solver for the electromagnetic fields and the electron density is particularly important. Since we will focus on the situation of strong laser pulses, the magnetic field is so small that it will be ignored. Therefore the vector potential, as the conjugate variable of the magnetic field, will also be removed from the Hamiltonian, which reduces TD-CDFT to TD-DFT. In this section, we summarize our work on the adaptive Finite Element Methods (FEM) [7,9–12] and spectral methods based on Frozen Gaussian Beams [13] for TD-DFT.

We first introduce some notations. $\Omega\subset\mathbb{R}^3$ denotes the computational domain, and the set $\mathcal{T}=\{\mathcal{K}_{j=1,2,\cdots,N_t}\}$ denotes a simplex partition of Ω in which $\mathcal{K}_j$ represents the j^{th} tetrahedral element in the mesh, where N_t denotes the total number of the tetrahedral

elements in the mesh. We assume that the mesh $\mathcal{T}$ covers the whole computational domain Ω, and that the intersection between two tetrahedronal elements is either empty or a common vertex or edge. On $\mathcal{T}$, a linear finite element space, $V_h=\{v|v\in C(\bar{\Omega})$, and $v|_{\mathcal{K}}\in \mathcal{P}_1, \forall \mathcal{K}\in\mathcal{T}\}$, is constructed for the space discretization of the Kohn-Sham equations, and will be used for both the ground state calculation and the time dependent simulation.

4.1 Adaptive methods for ground state Kohn-Sham equation

With the above notations, the discrete system of the Kohn-Sham equation (3.20) can be written as: to find $(\epsilon_j^h,\psi_j^h)\in\mathbb{R}\times V_h$ such that $\forall\phi\in V_h$,

$$\frac{\hbar^2}{2m}\big(\nabla\psi_j^h(\mathbf{r}),\nabla\phi(\mathbf{r})\big)+\big(v_{KS}(\mathbf{r})\psi_j^h(\mathbf{r}),\,\phi(\mathbf{r})\big)=\epsilon_j^h\big(\psi^h(\mathbf{r}),\,\phi(\mathbf{r})\big), \tag{4.1}$$

subject to

$$||\psi_j^h(\mathbf{r})||_2=1,\quad \psi_j^h(\mathbf{r})=0\quad \text{on }\partial\Omega, \tag{4.2}$$

for $j=1,2,\cdots,N_e$, where the Kohn-Sham effective potential $v_{KS}(\mathbf{r})$ has the same form as (3.21). LDA for the exchange-correlation functional is used for all simulations.

The main numerical issues on solving the above system include nonlinearity of the equation, nonlocality of the Hartree potential v_H, and the associated generalized eigenvalue problems. To deal with the nonlinearity, the popular Self-Consistent Field (SCF) iteration method is employed to linearize the system at each iteration. In the k^{th} iteration, the Hamiltonian H_0 is evaluated by using the current electron density $\rho_e^{(k)}$. Then the next wavefunctions, $\psi_{j=1,2,\cdots,N_e}^{(k+1)}$, are obtained by solving the derived linear eigenvalue system. To conduct efficient simulation for the nonuniform meshes and domains with complex geometry, instead of using the popular Fast Fourier Transform (FFT), we obtain v_H by solving the following Poisson equation equivalent to the original integral:

$$-\nabla^2 v_H(\mathbf{r})=4\pi e\rho_e(\mathbf{r}), \tag{4.3}$$

subject to $v_H(\mathbf{r})=0$, $||\mathbf{r}||\to\infty$. For accurate approximations of the above unbounded problem in Ω, the boundary value of the Hartree potential is given by a multipole expansion. And an algebraic multigrid method delivers a linearly scaled solver for the well defined Poisson system. A generalized eigenvalue problem $A\psi=\epsilon B\psi$ needs to be solved in each SCF iteration, and the quality of the eigensolver becomes crucial since it could affect the overall efficiency of the scheme. We employ the Locally Optimal Blocked Preconditioned Conjugate Gradient (LOBPCG) method together with the Gram-Schmidt orthogonalization to handle the eigenvalue problem, which has been proved to be effective in our study, even though the convergence of SCF can not be guaranteed for general cases. It is noted that the computational complexity of the Gram-Schmidt process is asymptotically quadratic with respect to N_e, which continuously motivates lots of work towards the (sub)linear scaling methods for large scale systems [44].

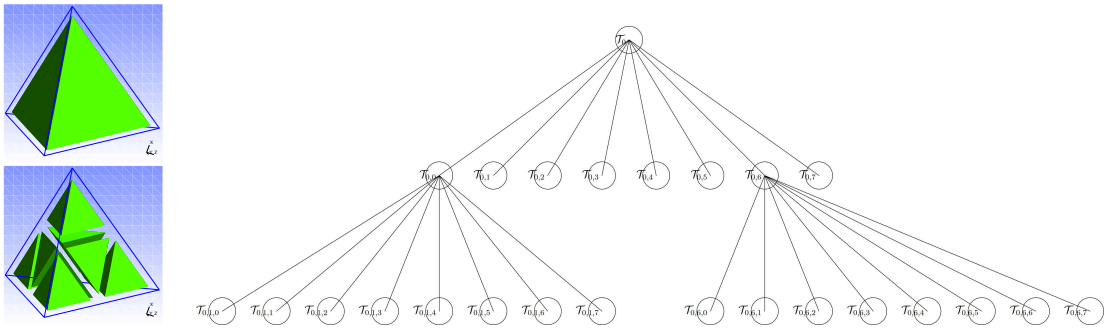

Figure 3: Left: Uniform refinement of a tetrahedron. Right: Octree tree for recording the mesh refinement.

Different from developing efficient numerical solvers for linear system obtained from uniform discretization, adaptive methods aim at generating efficient discretization for continuous equations, towards efficient simulations. In other words, adaptive methods try to use less mesh grids to build a discrete system whose solution is still sufficiently accurate. We have studied both *r*-adaptive method which relocates the mesh grids based on harmonic maps [10], and *h*-adaptive method which locally refines the mesh grids handled by a tree data structure [9]. In the following, we would summarize only our work on *h*-adaptive approach since our adaptive methods for TD-DFT is also based on *h*-adaptivity.

Two modules in a quality *h*-adaptive algorithm need to be designed carefully: i). local refinement and coarsening of the mesh grids, and ii). generation of the local error indicator. To handle the first module well, the so called Hierarchy Geometry Tree (HGT) originally proposed in [45] is employed in our algorithm. In three dimensional case, the realization of HGT is based on the octree structure in which each internal node exactly has eight children nodes. This coincides with the behavior of the uniform refinement of a tetrahedron very well that exactly eight sub-tetrahedron elements would be generated after the refinement, see Fig. 3 (left column). By the "refine when required" strategy, only two sub-tetrahedron elements may need to be further refined, and the tree would have the structure shown in Fig. 3 (right column), which corresponds to a nonuniform distribution of the mesh grids. By introducing two special tetrahedron elements [9], the potential issue on the hanging point can be handled well to preserve the finite element method conforming. The features of HGT include 1). the new mesh generation corresponds to the behavior of cutting tree and collecting all leaf nodes, which unifies the local refinement and coarsening of the mesh grids, 2). with the knowledge of the convergence rate of the numerical methods, the local error information can be assigned to every node in the tree, which enable us to fully take advantage of the error information, and 3). according to the tree structure, each pair of elements from two different meshes would have a belonging-to relation, allowing the efficient interpolation of the solution between two different meshes, which is very important in a dynamical simulation.

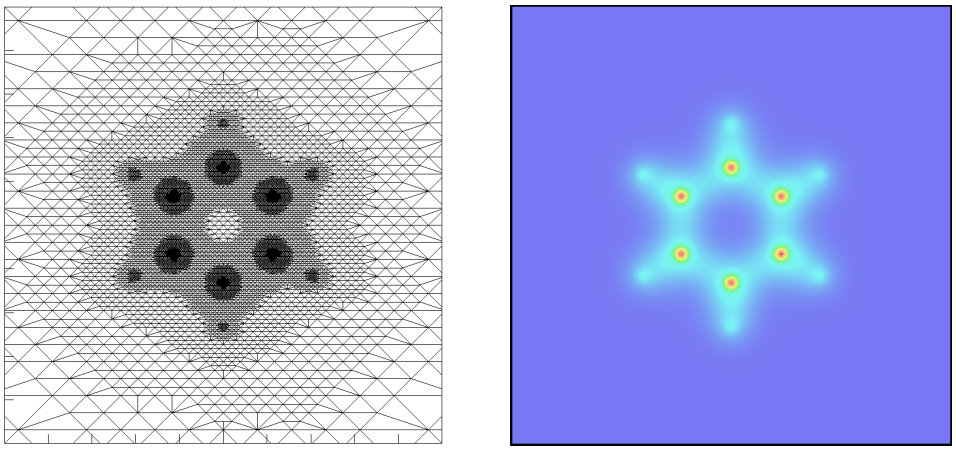

Figure 4: Ground state of a benzene molecule obtained with all electron calculation, in the vicinity of the molecule on the middle slice in the y-z plane.

Inspired by the work done by Verfürth in [46], the following residual type element-wise error indicator in solving the Kohn-Sham equation with the finite element methods is proposed [11, 12]:

$$\eta_{\mathcal{K}_j}^2 = \sum_k^{N_e} \left\{ \sum_e h_e ||\mathcal{J}_e(\psi_k^h)||_{2,e}^2 + h_{\mathcal{K}_j}^2 ||\mathcal{R}_{\mathcal{K}_j}(\psi_k^h)||_{2,\mathcal{K}_j}^2 \right\}, \tag{4.4}$$

where $\mathcal{J}_e(\psi_k^h) = \frac{1}{2}\left(\nabla\psi_k^h|_{\mathcal{K}_l}\cdot\vec{n}_{e,lj} + \nabla\psi_k^h|_{\mathcal{K}_j}\cdot\vec{n}_{e,jl}\right)$ denotes the jump of the flux across the common face e of $\mathcal{K}_j$ and its neighbor $\mathcal{K}_l$. $\vec{n}_{e,jl}$ and $\vec{n}_{e,lj}$ stand for the unit outward normals on the face e of $\mathcal{K}_j$ and $\mathcal{K}_l$, respectively. h_e is the diameters of the face e, while $h_{\mathcal{K}_j}$ is the diameter of the element $\mathcal{K}_j$. The second term $\mathcal{R}_{\mathcal{K}_j}(\psi^h)$ denotes the element residual of the equation, and has the following form on $\mathcal{K}_j$:

$$\mathcal{R}_{\mathcal{K}_j}(\psi_k^h) = \epsilon_k\psi_k^h + \frac{\hbar^2}{2m}\nabla^2\psi_k^h - V_{KS}\psi_k^h.$$

The translational and rotational variance of the total energy are common issues which affect the reliability of the simulations with real space methods such as Finite Difference Methods and Finite Element Methods. As illustrated in [12], the adaptive meshes can also help to alleviate this problem. To demonstrate the effectiveness of the proposed adaptive method, results on the all-electron calculation of the ground state of a benzene molecule are shown in Fig. 4. It is noted that the domain for this simulation is $[-100\ (a.u.), 100\ (a.u.)]^3$, and there are around 280,000 mesh grids in the domain. It can be observed easily from the figure that with the help of the error indicator (4.4), our adaptive method delivered a quality nonuniform mesh (Fig. 4, left) on which a quality electron density is also generated (same Fig. 4, right).

4.2 Adaptive simulations for time-dependent Kohn-Sham equation

The time-dependent Kohn-Sham (TDKS) density functional theory can be written as

$$\begin{aligned}\iota\hbar\frac{\partial\psi_j(\mathbf{r},t)}{\partial t} &= H_{KS}(\mathbf{r},t)\psi_j(\mathbf{r},t)\\ &= \left(-\frac{\hbar^2}{2m}\nabla^2+v_{KS}(\mathbf{r},t)+v_p\right)\psi_j(\mathbf{r},t),\end{aligned} \tag{4.5}$$

for j=1,2,$\cdots$,N_e, where $v_{KS}(\mathbf{r},t)$ is given in (3.15), and v_p denotes an external electric field. The difference between TD-DFT and TD-CDFT is that the magnetic field is not included in TD-DFT, therefore the vector potential as a conjugate variable of the magnetic field also does not exist in the Hamiltonian. For instance, in the study of the HHG, the external field is so strong that the magnetic field is ignored and $v_p = E_0 z f(t)\sin(\omega t)$ would be a time-dependent electric field term, where (E_0,ω,z) represent amplitude, frequency and direction of the electric field and $f(t)$ is an envelope function. When v_p is strong enough, the linear response TD-DFT would be no longer applicable. To solve (4.5) in the time domain, the equation needs to be fully discretized in time and space.

To satisfy properties such as unitary and time reversal symmetry, we employ the Crank-Nicolson scheme in [11] for time discretization such that

$$\left(\iota\hbar I-\frac{\Delta t}{2}H_{KS}\right)\psi_j^{n+1}=\left(\iota\hbar I+\frac{\Delta t}{2}H_{KS}\right)\psi_j^{n}, \tag{4.6}$$

for $j=1,2,\cdots,N_e$, where I is the identity matrix, and Δt denotes the size of the time step. Here H_{KS} is chosen as the average of the Hamiltonians at two adjacent time levels, i.e., $(H_{KS}^{n+1}+H_{KS}^{n})/2$. To handle the nonlinearity of the problem, a predication-correction procedure is introduced, and the initial H_{KS}^{n+1} is obtained with a forward Euler scheme. FEM is used for the spatial discretization of (4.5), and the adaptive module is introduced for partial resolving the efficiency issue. In the adaptive module, the HGT again is employed to handle the mesh refinement and coarsening. The difference compared with the adaptive module to the ground state Kohn-Sham equation is the local error indicator. In [11], the following elementwise error indicator is adopted

$$\begin{aligned}\eta_{\mathcal{K}_j}^2=\sum_k^{N_e}\Big\{ &\sum_{e\in\mathcal{K}_j}\frac{h_e\Delta t}{2}||\mathcal{J}_e(\psi_k^{real,n}+\psi_k^{real,n-1})||_{2,e}^2+h_{\mathcal{K}_j}^2\Delta t||\mathcal{R}_{\mathcal{K}_j}^{real}||_{2,\mathcal{K}_j}^2\\ &+\sum_{e\in\mathcal{K}_j}\frac{h_e\Delta t}{2}||\mathcal{J}_e(\psi_k^{img,n}+\psi_k^{img,n-1})||_{2,e}^2+h_{\mathcal{K}_j}^2\Delta t||\mathcal{R}_{\mathcal{K}_j}^{img}||_{2,\mathcal{K}_j}^2\\ &+\Delta t||\nabla(\psi_k^{real,n}-\psi_k^{real,n-1})||_{2,\mathcal{K}_j}^2+\Delta t||\nabla(\psi_k^{img,n}-\psi_k^{img,n-1})||_{2,\mathcal{K}_j}^2\Big\}.\end{aligned} \tag{4.7}$$

In the above formula, ψ^{real} and ψ^{img} stand for the real and imaginary parts of the complex-valued wavefunction ψ, i.e., $\psi=\psi^{real}+i\psi^{img}$. In [11], by splitting the real and imaginary

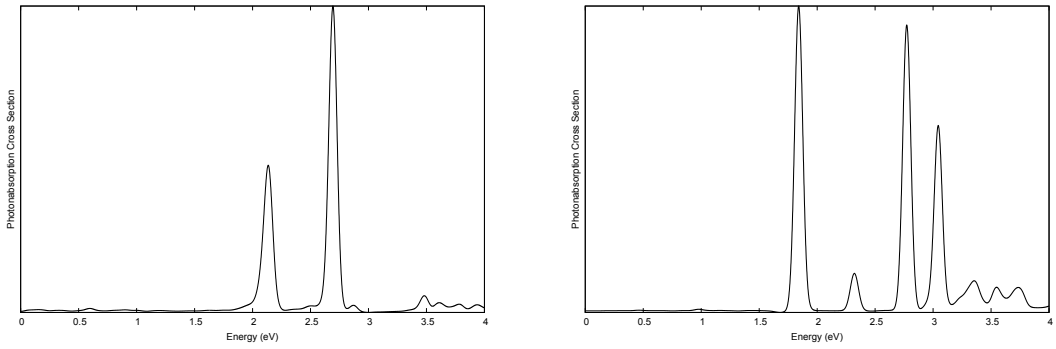

Figure 5: Photoabsorption spectra for Na_2 (left) and Na_4 (right) calculated with adaptive method. Please refer to [11] for detail.

parts of the wavefunction, the derived system consists of two equations, one for ψ^{real} and one for ψ^{img}. $\mathcal{R}^{real}$ and $\mathcal{R}^{img}$ in (4.7) are the residuals for both equations, respectively.

The mask function method is a popular way to prevent nonphysical reflections of the wavefunction from the boundary when the Dirichlet boundary is simply used in the simulation. However, the spectra shift can be observed from the results obtained by the mask function method when the domain size is small. This is easy to understand since absorbing layer defined by the mask function destroys the real dynamics of the electrons in the system. Adaptive methods have the advantage of greatly reducing the number of mesh grids needed to partition the large domain since the exponential decay of the wavefunction away from the ionic position. Hence, the straightforward idea of avoiding the nonphysical reflection of the wavefunction, i.e., using a sufficiently large computational domain, becomes possible at least for the simulations in the perturbative regime. For example, in [11] the photoabsorption spectra of Na_2 and Na_4 molecules are calculated with the pseudopotential. The domain is $[-100\ (a.u.), 100\ (a.u.)]^3$, and there are only around 3,200 mesh grids in this large domain. Results calculated with adaptive method shown in Fig. 5 coincides with the experimental ones [47] very well. It should be pointed out that when the external electric field is strong enough, the mask function becomes necessary since the oscillation of the wavefunction could be dramatic.

Besides the perturbative simulations such as the photoabsorption spectra calculation above, our time domain adaptive method can also be used to calculate the nonlinear phenomenon such as HHG. In [11], the dynamics of a lithium atom was studied under an external electric field $v_p = E_0 z f(t)\sin(\omega t)$ with the parameters $E_0 = 0.01\ (a.u.)$, $\omega = 0.03\ (a.u.)$. The envelope function is chosen as $f(t) = \sin^2(\pi t/T)$ with $T = 2\pi/(5\omega)$. In the result of dipole power spectra in Fig. 6 (top), those generated harmonic orders appear at the odd numbers, which agrees with theoretical result very well. Furthermore, a plateau profile can be observed after the initial exponential decay of the intensity, which also agrees with experiments. It is noted that the computational domain in this simulation is $[-150\ (a.u.),150\ (a.u.)]^3$, while the peak value of the number of the mesh grids

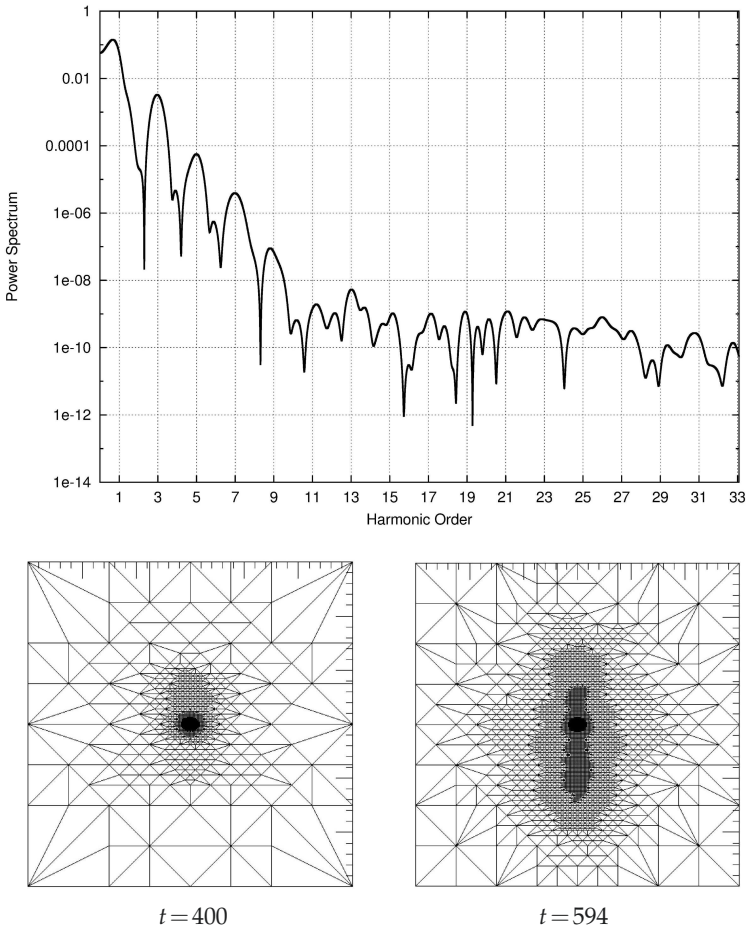

Figure 6: High harmonic generation for a lithium atom. Top: dipole power spectrum; Bottom: meshes at different time instant. Please refer to [11] for detail.

during the dynamic simulation is around 1.1×10^5. With the adaptive method, there is a very significant reduction on the mesh grid in our simulation, compared with a similar numerical experiment in [48]. Fig. 6 (bottom) shows the different meshes at different time instants.

4.3 A spectral algorithm for the time-dependent Kohn-Sham equations

In [13], we develop a novel spectral method for solving the time-dependent Kohn-Sham (TDKS) equations in the semiclassical regime, where the propagator is derived using a Fourier integral operator commonly known as the Frozen Gaussian approximation (FGA). In the case of laser potentials, we derived a simplified FGA to avoid the high dimensional integration.

The nonlinear TDKS equation is solved self-consistently using a predictor-corrector algorithm through the following linear Schrödinger equation:

$$\mathrm{i}\hbar\partial_t\phi = -\frac{\hbar^2}{2m}\nabla^2\phi + V(\boldsymbol{r},t)\phi, \qquad \phi_0(\boldsymbol{r}) \in L^2(\mathbb{R}^3), \tag{4.8}$$

which we will be solving with the first order FGA ansatz:

$$\phi_{\mathrm{FGA}}(\boldsymbol{r},t) = \frac{1}{(2\pi\hbar)^{9/2}}\int_{\mathbb{R}^9} A(t,\boldsymbol{q},\boldsymbol{p}) G_{\boldsymbol{Q},\boldsymbol{P}}(\boldsymbol{r}) e^{\mathrm{i}S(t,\boldsymbol{q},\boldsymbol{p})/\hbar}\overline{G}_{\boldsymbol{q},\boldsymbol{p}}(\boldsymbol{r}')\phi_0(\boldsymbol{r}')\,d\boldsymbol{r}'\,d\boldsymbol{q}\,d\boldsymbol{p}, \tag{4.9}$$

where $G_{\boldsymbol{q},\boldsymbol{p}}(\boldsymbol{r})$ are Gaussian functions depending on phase space coordinates $(\boldsymbol{q},\boldsymbol{p})$:

$$G_{\boldsymbol{q},\boldsymbol{p}}(\boldsymbol{r}) = \exp\left(-\frac{1}{2\hbar}|\boldsymbol{r}-\boldsymbol{q}|^2 + \mathrm{i}\frac{\boldsymbol{p}}{\hbar}\cdot(\boldsymbol{r}-\boldsymbol{q})\right).$$

Compared with the WKB method and the traditional Gaussian Beam method, FGA avoids the breakdown of the solution where the corresponding Hamilton-Jacobi equation develops singularities [49] and the splitting of beams [50]. The Gaussian functions in phase space are propagated using the Hamiltonian flow:

$$\begin{aligned}\frac{d\boldsymbol{Q}}{dt} &= \boldsymbol{P},\\ \frac{d\boldsymbol{P}}{dt} &= -\nabla_{\boldsymbol{Q}}V(\boldsymbol{Q}),\end{aligned}$$

and the equations for the phase S and amplitude a are given by:

$$\begin{aligned}\frac{dS}{dt} &= \frac{1}{2}|\boldsymbol{P}|^2 - V(\boldsymbol{Q}),\\ \frac{da}{dt} &= \frac{a}{2}\mathrm{tr}\left((\partial_{\boldsymbol{z}}\boldsymbol{P} - \mathrm{i}\partial_z\boldsymbol{Q}\nabla^2_{\boldsymbol{Q}}V)Z^{-1}\right),\end{aligned}$$

with $Z := \partial_{\boldsymbol{z}}(\boldsymbol{Q}+\mathrm{i}\boldsymbol{P})$ and $\partial_{\boldsymbol{z}} := \partial_{\boldsymbol{q}} - \mathrm{i}\partial_{\boldsymbol{p}}$.

For the case of laser potentials $V(\boldsymbol{r},t) = \boldsymbol{\alpha}\cdot\boldsymbol{r}f(t)$, the FGA can be further simplified, thereby efficiently evaluated by Fast Fourier Transforms (FFT). The absorbing boundary conditions for ionization also becomes trivial as Gaussian functions have standard deviation $\mathcal{O}(\sqrt{\epsilon})$ and smoothly decay to zero.

We apply our FGA-based algorithm for a system of 57 valence 1 electron atoms separated at a distance of 4 (a.u.) and arranged in a stable face centered cubic configuration. The the full xc-potential is replaced by the pseudopotential of the form:

$$v_0(\boldsymbol{r}) = \sum_{i=1}^{57}\frac{-1}{\sqrt{1+|\boldsymbol{r}-\boldsymbol{R}_i|^2}},$$

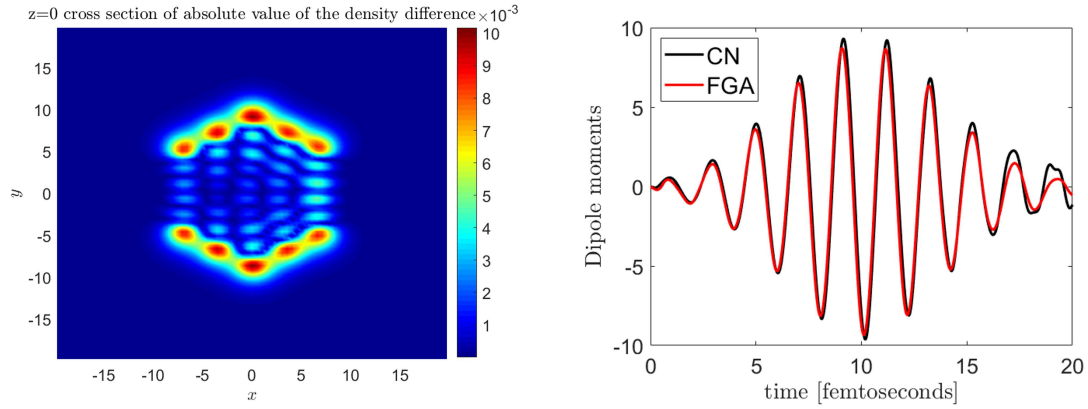

Figure 7: Comparison of the FGA-based algorithm and the Crank-Nicolson finite difference scheme. Left: $z=0$ cross section of difference in densities. Right: Dipole moments

and the external potential is chosen to be

$$v_{ext}(\mathbf{d}r,t)=x.$$

Our reference solution is computed using the Crank-Nicolson scheme with a large spatial domain and small time steps. As can be seen by the Fig. 7, the densities differ the most near the location of the nuclei, as a result of the smoothness of our spectral method. The system is then propagated using the Gaussian pulse external field:

$$v_{Ext}(\boldsymbol{r},t)=Ax\exp\left(-(t-827/2)^2/(2\sigma)\right)\cos\left(\omega(t-827/2)\right).$$

The result on the dipole moments is shown in Fig. 7. Generally the domain size for our type of spectral method needs to be large enough so that a significant part of the orbitals do not leave the domain.

5 Current and future work

The ongoing research efforts include the theoretical investigation of the Maxwell-Kohn-Sham (MKS) system, improving the current numerical schemes, and applications to complex practical systems.

5.1 Rigorous analysis of the MKS system and the multiscale scheme

Understanding of regularity and long time behaviors of solutions for the coupled Maxwell-Kohn-Sham system is vital for developing efficient and stable numerical methods. For a single particle system, the global well-posedness of the Maxwell-Schrödinger system has been previously established in [51]. Recent progress on the regularity of the weak solution for the time dependent Kohn-Sham has been made in [53]. The analysis of

the multiscale scheme will also shed light on discovering new mathematical techniques for the investigation of nano scale structures where multiscale effects and multiscale challenges are dominant. Robust and accurate algorithms for related non-linear eigenvalue problems will also be studied.

5.2 Applications to novel nano devices

Real time simulation of coupled Maxwell's equations and TD-DFT has been successfully applied in the investigation of the absorption spectrum of the N3 dye molecule and the Raman spectrum of pyridine, under surface plasmonic enhancement by silver nano particles [54]. Recent progress has also been made on time domain simulation of coupled Ehrenfest molecular dynamics and TD-DFT [52, 55]. Incorporating all scales by the full coupling of Maxwell's equation, Ehrenfest molecular dynamics and TD-DFT will be helpful to understand transition pathways of light driven nano devices and optimal designing of such systems, which also poses significant challenges both for simulation and analysis. Efficient adaptive FEM will be applied to study High order Harmonic Generations (HHG) and Metallic structures, which can be achieved by combining with recent advances in parallel transport Crank-Nicolson (PT-CN) scheme that can significantly increase the time step for real-time TDDFT [56].

Acknowledgments

The research program was supported by NSF-DMS FRG 0968360. The work of G. Bao was supported in part by a NSFC Innovative Group Fund 11621101. G. Hu's research was supported NSFC-11871489. D. Liu's and R. Delgadillo's research programs were supported by NSF-DMS 1720002. S. Luo's research was supported by NSF-DMS 1719907.

References

[1] G. Bao and M. I. Weinstein, *Mathematical Challenges and Opportunities in Optics and Photonics*, SIAM News, May 2015.
[2] C. Cohen-Tannoudji, J. Dupont-Roc and G. Grynberg, *Photons and Atoms: Introduction to Quantum Electrodynamics*, Wiley, New York, 1989.
[3] K. Cho, *Optical Response of Nanostructures: Microscopic Nonlocal Theory*, Springer, New York, 2003.
[4] O. Keller, *Local fields in the electrodynamics of mesoscopic media*, Phys. Rep., 268, 85-262, 1996.
[5] A. Stahl and I. Balslev, *Electrodynamics of the Semiconductor Band Edge*, Springer Tract in Mod. Phys. 110, Springer-Verlag, New York, 1987.
[6] G. Bao, G. Hu, D. Liu and S. Luo, *Multi-physical modeling and multi-scale computation of nano optical responses*, Recent Advances in Scientific Computing and Applications, Contemp. Math., 586, 43-55, 2013.
[7] G. Bao, D. Liu and S. Luo, *A multiscale method for optical responses of nano structures*, SIAM Applied Math., 73, 741-756, 2013.

[8] G. Bao, D. Liu and S. Luo, *Multiscale modeling and computation of light driven nano devices*, J. Comp. Phys., 316, 558-572, 2016.
[9] G. Bao, G. Hu and D. Liu, *An h-adaptive finite element solver for the calculations of the electronic structures*, J. Comp. Phys., 231, 4967-4979, 2012.
[10] G. Bao, G. Hu and D. Liu, *Numerical solution of the Kohn-Sham equation by finite element methods with an adaptive mesh redistribution technique*, J. Sci. Comput., 55, 372-391, 2013.
[11] G. Bao, G. Hu and D. Liu, *Real-time adaptive finite element solution of time dependent Kohn-Sham equation*, J. Comp. Phys., 281, 743-758, 2015.
[12] G. Bao, G. Hu and D. Liu, *Towards translational invariance of total energy with finite element methods for Kohn-Sham equations*, Comm. Comp. Phys., 19, 1-23, 2016.
[13] R. Delgadillo and D. Liu, *A spectral algorithm for the time-dependent Kohn-Sham equations: Accurately treating external potentials based on frozen Gaussian approximations*, SIAM Scientific Computing, 42, B656-B674, 2020.
[14] S. Ghosh and A. Dhara, *Density-functional theory of many-electron systems subjected to time dependent electric and magnetic fields*, Phys. Rev. A, 38, 1149-1158, 1998.
[15] P. Hohenberg and W. Kohn, *Inhomogeneous electron gas*, Phys. Rev., 136, B864-B871, 1964.
[16] E. Runge and E. Gross, *Density-functional theory for time dependent systems*, Phys. Rev. Lett., 52, 997-1000, 1984.
[17] W. Kohn and L. Sham, *Self-consistent equations including exchange and correlation effects*, Phys. Rev., 140, 1133-1138, 1965.
[18] G. F. Bertsch, J. I. Iwata, A. Rubio and K. Yabana, *Real-space, real-time method for the dielectric function*, Phys. Rev. B, 62, 7998-8002, 2000.
[19] N. T. Maitra, I. Souza and K. Burke, *Current-density functional theory of the response of solids*, Phys. Rev. B, 68, 045109, 2003.
[20] W. E and J. Lu and X. Yang, *Effective Maxwell equations from time dependent density functional theory*, Acta Mathematica Sinica, 27, 339-368, 2011.
[21] L. Prechtel, L. Song, S. Manus, D. Schuh, W. Wegscheider and A. W. Holleitner, *Time-resolved picosecond photocurrents in contacted carbon nanotubes*, Nano Lett., 11, 269-272, 2011.
[22] I. Willner and S. Rubin, *Control of the structure and functions of biomaterials by light*, Angew. Chem. Int. Ed., 35, 367-385, 1996.
[23] P. Gorostiza and E. Isacoff, *Optical switches for remote and noninvasive control of cell signaling*, Science, 322, 395-399, 2008.
[24] Q. Yuan, Y. Zhang, Y. Chen, R. Wang, C. Du, E. Yasun and W. Tan, *Using silver nanowire antennas to enhance then conversion efficiency of photo responsive DNA nanomotors*, Proc. Natl. Acad. Sci., 108, 9331-9336, 2011.
[25] L. Qiu, C. Wu, M. You, D. Han, T. Chen, G. Zhu, J. Jiang, R. Yu and W. Tan, *A targeted, self-delivered and photocontrolled molecular beacon for mRNA detection in living cells*, J. Am. Chem. Soc., 135, 12952-12955, 2013.
[26] T. Wu, T. A. Nieminen, S. Mohanty, J. Miotke, R. L. Meyer, H. Rubinsztein-Dunlop and M. W. Berns, *A photon-driven micro motor can direct nerve fibre growth*, Nature Photonics, 6, 62-67, 2012.
[27] T. Zhang, H. Chang, Y. Wu, P. Xiao, N. Yi, Y. Lu, Y. Ma, Y. Huang, K. Zhao, X. Yan, Z. Liu, J. Tian and Y. Chen, *Macroscopic and direct light propulsion of bulk graphene material*, Nature Photonics, 9, 471-477, 2015.
[28] M. Hentschel, R. Kienberger, C. Spielmann, G. A. Reider, N. Milosevic, T. Brabec, P. Corkum, U. Heinzmann, M. Drescher and F. Krausz, *Attosecond metrology*, Nature, 414, 509-513, 2001.
[29] M. Drescher, M. Hentschel, R. Kienberger, M. Uiberacker, V. Yakovlev, A. Scrinzi, T. West-

erwalbesloh, U. Kleineberg, U. Heinzmann and F. Krausz, *Time-resolved atomic inner-shell spectroscopy*, Nature, 419, 803-807, 2002.
[30] M. A. L. Marques, N. T. Maitra, F. M. S. Nogueira, E. K. U. Gross and A. Rubio ed., *Fundamentals of Time dependent Density Functional Theory*, Springer Heidelberg, 2012.
[31] C. A. Ullrich, *Time dependent Density-Functional Theory*, Oxford University Press, New York, 2012.
[32] M. L. Brongersma and V. M. Shalaev *The case for plasmonics*, Science, 328, 440-441, 2010.
[33] W. U. Huynh, J. J. Dittmer and A. P. Alivisatos, *Hybrid nanorod-polymer solar cells*, Science, 295, 2425-2427, 2002.
[34] S. A. Maier, P. G. Kik, H. A. Atwater, S. Meltzer, E. Harel, B. E. Koel and A. G. Requicha, *Local detection of electromagnetic energy transport below the diffraction limit in metal nanoparticle plasmon waveguides*, Nature Materials, 2, 229-232, 2003.
[35] G. Zhu, M. Mayy, M. Bahoura, B. A. Ritzo, H. V. Gavrilenko, V. I. Gavrilenko and M. A. Noginov, *Elongation of surface plasmon polariton propagation length without gain*, Opt. Exp., 16, 15576-15583, 2008.
[36] G. Y. Panasyuk, J. C. Schotland and V. A. Markel, *Theoretical and numerical investigation of the size dependent optical effects in metal nanoparticles*, Phys. Rev. B, 84, 155460, 2011.
[37] D. Marx and J. Hutter, *Ab Initio Molecular Dynamics*, Cambridge University Press, Cambridge, 2009.
[38] S. H. Vosko, L. Wilk and M. Nusair, *Accurate spin dependent electron liquid correlation energies for local spin density calculations: A critical analysis*, Can. J. Phys., 58, 1200-1211, 1980.
[39] G. Vignale and W. Kohn, *Current dependent exchange-correlation potential for dynamical linear response theory*, Phys. Rev. Lett., 77, 2037-2040, 1996.
[40] M. E. Casida, *Time dependent density functional response theory for molecules*, Recent Advances in Density Functional Methods, 155-193, D. P. Chong (Ed.), World Scientific, Singapore, 1995.
[41] M. van Faassen, P. L. de Boeij, R. van Leeuwen, J. A. Berger and J. G. Snijders, *Ultranonlocality in time dependent current-density-functional theory: Application to conjugated polymers*, Phys. Rev. Lett., 88, 186401-186404, 2002.
[42] A. D. Rakić and A. B. Djurišić and J. M. Elazar and M. L. Majewski, *Optical properties of metallic films for vertical-cavity optoelectronic devices*, Appl. Opt., 22, 5271-5283, 1998.
[43] J. M. Jin, *The Finite Element Method in Electromagnetics*, 2nd Ed., New York: John Wiley & Sons, 2002.
[44] C. J. García-Cervera, J. Lu and W. E, *A sub-linear scaling algorithm for computing the electronic structure of materials*, Commun. Math. Sci., 5, 999-1026, 2007.
[45] R. Li, *On multi-mesh h-adaptive algorithm*, J. Sci. Comput., 24, 321-341, 2005.
[46] R. Verfürth, *A Posteriori Error Estimation Techniques for Finite Element Methods*, ISBN:9780199679423, Oxford University Press, 2013.
[47] I. Vasiliev, S. Öğüt and J. R. Chelikowsky, *First-principles density-functional calculations for optical spectra of clusters and nanocrystals*, Phys. Rev. B, 65, 115416, 2002
[48] E.P. Fowe and A.D. Bandrauk, *Nonlinear time-dependent density-functional-theory study of ionization and harmonic generation in CO2 by ultrashort intense lase pulses: orientational effects*, Phys. Rev. A, 81, 023411, 2010
[49] G. Panati, H. Spohn and S. Teufel, *Effective dynamics for Bloch electrons: Peierls substitution and beyond*, Comm. Math. Phys. 242, 547-578, 2003.
[50] M. M. Popov, *A new method of computation of wave fields using Gaussian beams*, Wave Motion, 4, 85-97, 1982.
[51] D. Tataru and I. Bejenaru, *Global wellposedness in the energy space for the Maxwell-Schrödinger*

system, Comm. Math. Phys., 288,145-198, 2009.

[52] Z. Wang, S. S. Li and L. W. Wang, *Efficient real-time time-dependent density functional theory method and its application to a collision of an ion with a 2D material*, Phys. Rev. Lett., 114, 063004, 2015.

[53] J. W. Jerome, *Time dependent closed quantum systems: Nonlinear Kohn-Sham potential operators and weak solutions*, J. Math. Anal. Appl., 429, 995-1006, 2015.

[54] H. Chen, J. M. McMahon, M. A. Ratner and G. C. Schatz, *Classical electrodynamics coupled to quantum mechanics for calculation of molecular optical properties: A RT-TDDFT/FDTD approach*, J. Phys. Chem. C, 114, 14384-14392, 2010.

[55] G. Kolesov, O. Granas, R. Hoyt, D. Vinichenko and E. Kaxiras, *Real-time TD-DFT with classical ion dynamics: Methodology and applications*, J. Chem. Theory Comput., 12, 466-476, 2016.

[56] W. Jia, L.-W. Wang and L. Lin, *Fast real-time time-dependent density functional theory calculations with the parallel transport gauge*, J. Chem. Theory Comput., 14, 5645, 2018.